ANALYSIS OF PORTO DA CALADA MAGNETIZATION

Fieldwork and Laboratory Analysis Report

MASTER DEGREE IN GEOPHYSICAL SCIENCES

GEOMAGNETISM

Ana Caldeirinha
Liliana Oliveira
Susana Silva

June 21ST 2016

Contents

Figure List

Table List

1. Introduction

The Jurassic–Cretaceous boundary is still poorly understood and is the last system boundary without a Global Boundary Stratotype Section and Point (GSSP). Furthermore, biostratigraphic correlations among palaeobiogeographical provinces are hampered by barriers to faunal exchange (e.g., Ogg et al. 2012). Dating by magnetostratigraphy coupled with regional correlations and biostratigraphy has been successfully used to make large-scale correlations. Earlier studies have placed the Tithonian–Berriasian boundary in various different positions, but currently the base of Chron M18r is assigned and is even a candidate as a correlation event marking the boundary (Ogg et al. 2012). The onshore uppermost Jurassic to lowermost Cretaceous of the Lusitanian Basin (Western Portugal, see Figure 1 (right)) has been the subject of numerous studies (Ramalho 1971; Rey 1972, 1993; Mateus 2006; Dinis et al. 2008; Myers et al. 2012). It includes several good exposures of the Jurassic–Cretaceous (J–K) transitions, for example, Porto da Calada, the Sintra–Cascais region, and Praia dos Lagosteiros–Cabo Espichel. Despite the favorable exposure, the exact position of the J–K boundary is poorly known, due to the lack of good biostratigraphic markers in a complex stratigraphy, which records important variations in a coastal landscape that was still under the influence of the late Oxfordian to early Kimmeridgian rifting (Salminen et al., 2013).

In the magnetostratigraphic study recently conducted in the Porto da Calada section performed by Salminen et al. (2013), they present a stratigraphic log supporting a preliminary magnetostratigraphy of a Tithonian–Berriasian section in Porto da Calada and locate the Tithonian–Berriasian boundary based on biostratigraphy and reversed and normal magnetostratigraphy.

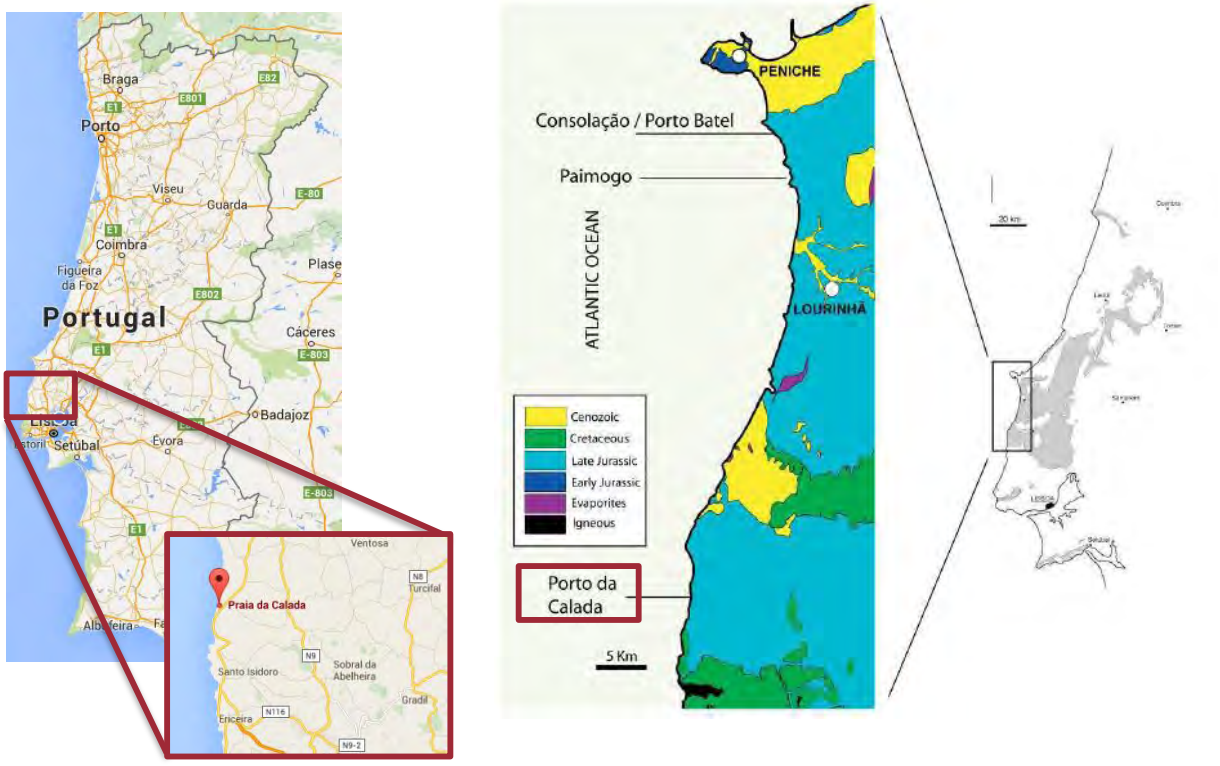

Figure 1. Location of Porto da Calada beach (left) and simplified geological map of the central west coast of Portugal (right); Upper Jurassic in grey at the right.

The aim of this study is to determine the nature of magnetization of the rock samples collected in the Porto da Calada section (39.04°N, 9.41°W), located at 10 km of Ericeira village, Mafra (Figure 1), in order to verify the existence of inversions in Earth's magnetic field.

We performed this study in the Porto da Calada section because it is a Portuguese reference section of the Lusitanian Basin (Western Portugal): it is the main stratigraphic reference of the geological period Tithonian–Berriasian, dated at ~140 Myr, and provides an excellent record of the Late Jurassic-Lower Cretaceous time interval, with extensive outcrops and in the recently found dinosaur bones.

Figure 2. Porto da Calada section.

To study the magnetization nature, several samples were collected in Porto da Calada beach (Section 3). These samples were then taken to the laboratory where they were cut into standard paleomagnetic specimens, which then have been treated using alternating field (AF) (Section 4). We performed a data analysis (Section 5) and then discussed the results (Section 6). The next topic explains some of the concepts and the key points which are necessary for a better understanding of this work.

2. Theoretical Principles[1]

It is known for a very long time that the Earth has a magnetic field. It allows the deflection of most of the solar wind, protecting the surface from dangerous ultraviolet radiation, and it is very useful for navigation, just to name a few examples on the importance of the Earth's magnetic field.

The conceptual model for the present geomagnetic field is that of an inclined dipole, which has an angle of approximately 11.5º with respect to the Earth's rotation axis (consistent with the geographic poles), as shown in Figure 1. The two dipolar components (north and south) are called geomagnetic poles. These are defined as points in the surface where extensions of the inclined dipole intersect the Earth's center.

The magnetic (or dip) poles do not coincide with the geomagnetic ones, as was expected if the geomagnetic field was in fact fully explained by a geocentric dipole. As this is not the case (it only explains 90% of the total magnetic field), the position of the dipole was refined and allowing for its position to best fit the field. This resulted in a dipole positioned about 500 km from the center of the Earth, toward the northwestern portion of the Pacific Basin. This difference is explained by a nondipolar portion of the geomagnetic field, due to the activity of the sun on the ionosphere and magnetosphere.

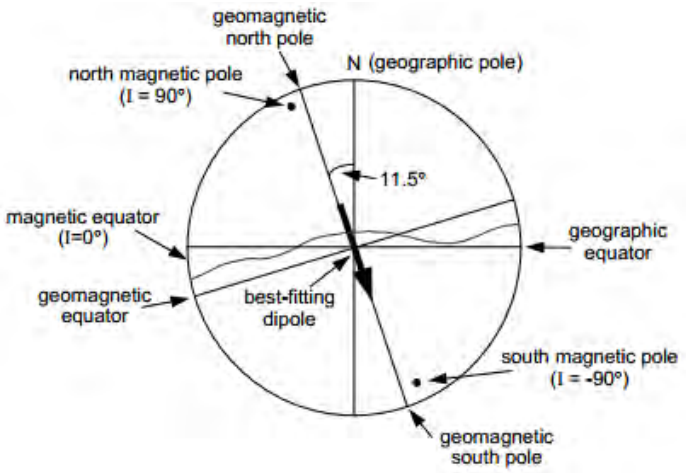

Figure 3. Inclined geocentric dipole model Butler, R. (2004).

A magnetic field, such as the Earth's, is characterized by its magnitude (*F,* proportional to the force the field exerts on a magnetic material) and direction (Figure 2). In turn, the latter can be described by the declination (*D,* angle between the geographic north and the magnetic north) and inclination (*I,* angle between the vertical component of the magnetic field and the horizontal plane, varying between -90º and 90º).

[1] This section is based on Butler, R. (2004), Miranda, J. M. (2009), Neres, M. (2013) and Font, E. works.

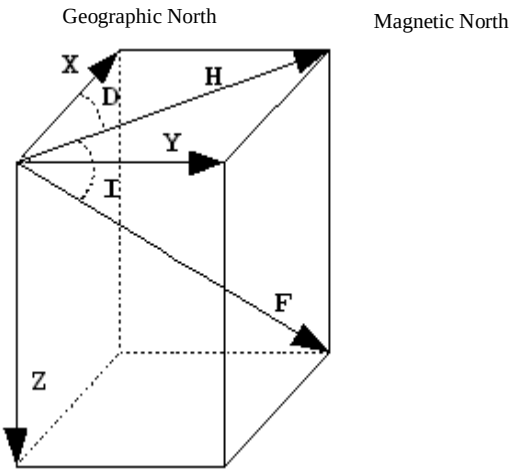

Figure 4. Representation of the magnetic field components in a coordinate system.
H - Horizontal component of the field; F – intensity of the magnetic field. Redrawn after IPMA.

It has been observed that the direction and magnitude of the geomagnetic field changes over time. It may suffer variations over a short period of time, such as *aurora borealis* and magnetic pulses, or for longer periods, namely the geomagnetic secular variation, with periods longer than a year. It is also known that the dipole switches polarity, evident by cores taken from deep ocean floors. Information about the past geomagnetic field can be found through analysis of rocks samples and is one of the key topics in paleomagnetism studies.

Magnetization has essentially two components: induced ($\chi \boldsymbol{H}$, exists in the presence of an ambient magnetic field) and remanent ($\boldsymbol{M}^R$, recording of magnetic fields that have acted on the material). Magnetization is determined as in Equation x:

$$\boldsymbol{M} = \chi \boldsymbol{H} + \boldsymbol{M}^R$$

The magnetic susceptibility - χ, is the capability of a material to respond to an applied magnetic field. Thus, rocks with different mineralogical composition will have a different behavior towards the same magnetic field. There are three types of magnetic behavior: diamagnetism, paramagnetism and ferromagnetism. Each respective atomic coupling is presented in Figure 3.

Diamagnetic materials have negative susceptibility, i.e. the magnetization induced by the field has an opposite direction to that of the magnetic field. The magnetization of these types of materials is weak, and when the applied field is removed, it reduces to zero, as it is linearly dependent of the magnetic field. Furthermore, the susceptibility is independent of temperature. Even though all matter is diamagnetic, as diamagnetism is very weak, it is overwhelmed by the other magnetic behaviors. Thus, it is only dominant on few materials, such as quartz and calcite.

A material is paramagnetic when its magnetic susceptibility is positive and inversely proportional to the temperature, as the induced magnetization on the material has the same direction as the applied field. In the absence of a magnetic field, its atoms are randomly oriented, while under the applied field, their magnetic moments tend to align. If the field is removed, however, as the

magnetic moments are independent, any small thermal perturbation will cause them to be randomly distributed, and thus, the resultant magnetization will be null. Olivines and pyroxenes, for example, have paramagnetic behavior.

Unlike the two magnetic behaviors presented previously, a ferromagnetic material (such as iron, cobalt or nickel) is characterized by a very strong magnetization, due to the interaction between magnetic moments. In case a direct parallel coupling between adjacent magnetic moments exists, the material is ferromagnetic. If, on the other hand, the coupling is antiparallel with equal magnetic moment, thus resulting in a null net magnetization, the material is antiferromagnetic. This happens in substances like manganese (II) oxide and ferrous oxide. There is also ferrimagnetism, in which magnetic moments are antiparallel, as in antiferromagnetism, except the magnitudes of moments are unequal, and as a result there is a significant net magnetic moment. Magnetite, titanomagnetite and pirrotite are examples of ferrimagnetic minerals.

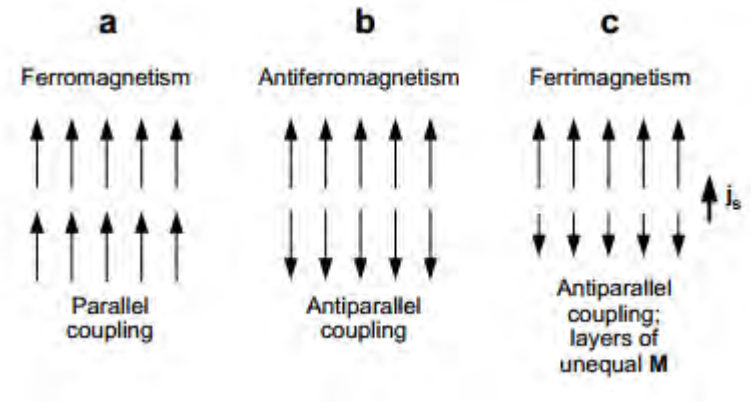

Figure 5. Couplings for (a) ferromagnetic, (b) antiferromagnetic, and (c) ferrimagnetic materials. j_s stands for the net magnetization Butler, R. (2004).

Distance between atoms in a material increases during thermal expansion, thus weakening the coupling between magnetic moments. This means that even if a material is ferromagnetic, there is a certain temperature at which interatomic distance has increased to the point at which that coupling is destroyed. This is called the Curie temperature (or Néel temperature, in case the material is antiferromagnetic). Above that temperature, the magnetic moments are no longer dependent and the material becomes paramagnetic. However, in most cases, this process is reversible if the material is cooled below its Curie temperature, and magnetic minerals are remagnetized, as they are continually induced by the ambient magnetic field. Through this process, they gain a viscous remanent magnetization (VRM), i.e., a magnetization component with the same direction as the geomagnetic field of the time. On the other hand, the blocking temperature is the temperature above which the net magnetization will vanish. This propriety depends on the grain and not the mineral constituting it.

In the presence of natural ambient fields, materials acquire a natural remanent magnetization (NRM). When acquired during rock formation it is called primary NRM, which is the component required for most paleomagnetic studies, as it can record the geomagnetic field of the time the

rock was formed and may even retain that information over geological time scales. NRM can also be acquired after the formation of the rock and may alter the primary NRM. It is, therefore, called secondary NRM. Thus, the total NRM is given by these two components.

When a ferromagnetic material with a null net magnetic moment is exposed to an applied field, its magnetization will increase. If the magnetic field has low intensity, this process will be reversible. If, however, the material is exposed to strong magnetizing fields in a short period of time (some seconds) and at constant temperature, the process becomes irreversible and when the field is removed what remains is the isothermal remanent magnetism (IRM). Moreover, if all the magnetic moments align with the maximum applied field, the remanence acquired is the saturation isothermal remanence magnetization (sIRM). These processes can be represented by a hysteresis curve such as the one in Figure 6.

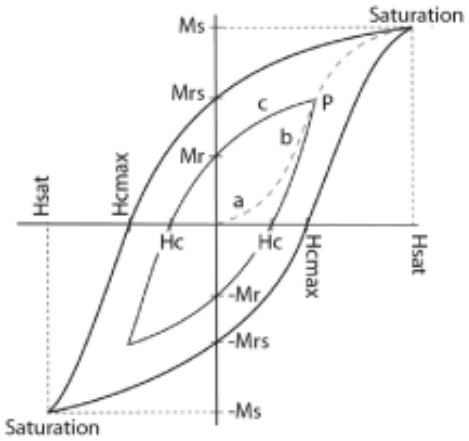

Figure 6. Hysteresis curve and main hysteresis parameters. M_s – saturation magnetization; M_{rs} – saturation remanent magnetization. From Neres M. (2013).

In SD (single-domain) particles, the remanent magnetization is given by:

$$J_r(t) = J_{ro}e^{-\frac{t}{\tau}}$$

With τ being the relaxation time, the time that the magnetization of the mineral takes to be reduced to a factor of 1/e.

Through AF demagnetization, the sample under study is exposed to an alternating magnetic field, and allows the determination of the NRM directions, i.e., the directions of the magnetization recorded in the rock sample at the time it was formed. The maximum value of the AF demagnetizing field is H_{AF}, and the waveform of the alternating magnetic field is a sinusoid with linear decrease in magnitude with time, as the one in Figure 7.

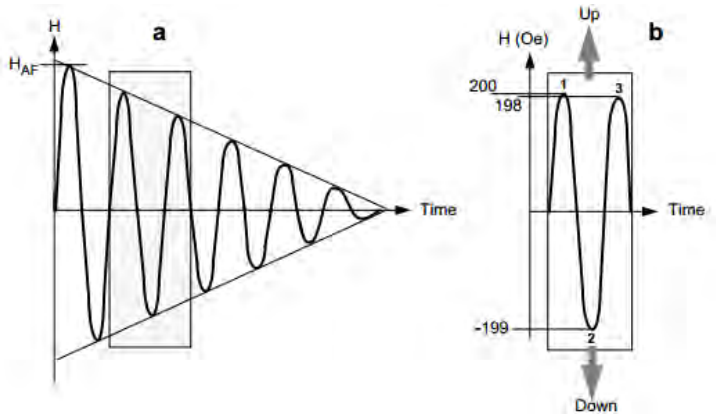

Figure 7. Schematic representation of AF demagnetization. From Butler, R. (2004).

Most instruments allow AF demagnetization to maximum H_{AF} of 100 mT, such as the one used in this work. The procedure involves a step-by-step measuring of the NRM till the field reaches the value of H_{AF} (in this case, 100 mT). The response of the AF treatment depends on the coercivity (h_c) of the ferromagnetic minerals present in the sample. As Figure 7 shows, the magnetic moments of all the grains with $h_c \leq 20$ mT align towards "up" and those with $h_c \leq 19.9$ mT align towards "down". The process continues with a value of 19.8 mT. In the end, the magnetic moments will be cancelled. The contribution of all the grains which $h_c \leq H_{AF}$ is therefore destroyed and only the NRM carried by the grains which $h_c > H_{AF}$ is preserved.

Understanding the concepts described in this section is fundamental for paleomagnetic studies of rock samples, through which it is possible to obtain past configurations of the geomagnetic field, which is the main focus of this work.

3. Geological Setting

The Porto da Calada section (39.04°N, 9.41°W), located at 10 km of Ericeira village, Mafra, is a section with approximately 43 meters in thickness.

The Porto da Calada Formation was formally defined by Rey (1993). It is laterally equivalent to the north and to the east to the fluvial Serreira Formation and to the south, in the Sintra region, to the limestones and marls with *Anchispirocyclina lusitanica, Mantelliana purbeckensis* and *Trocholina*, including the "nankeen-yellow limestone levels" ("Infravalanginian"). It corresponds to the top of the Farta Pão Formation and to the uppermost part of the Feixial unit, considered as a formation by Leinfelder (1986) and as a member of the Farta Pão Formation by Fürsich et al. (2009). It is equivalent to the lower part of the "Hauterivian and Valanginian" of Zbyszewski et al. (1955) to the NE.

In the Porto da Calada section, the unit was studied by Rey (1972, 1993) and Salminen et al. (2013). It is dominated by cross-bedded sandstones, often conglomeratic, with minor mudstones. The sandstone bodies usually show lateral accretion sigmoids, sometimes heterolithic, and include several amalgamated channels; reworked calcrete nodules forms breccia-like conglomerates at the base of the larger channels. The overbank mudstones include frequent laminae of fine sandstone and calcrete levels. The carbonate levels are micritic limestone with gastropods and bivalves, and dolomitic facies, including thin nodular yellowish beds at the top. Several limestone levels along the unit shows the large foraminifera *Anchispirocyclina lusitanica*.

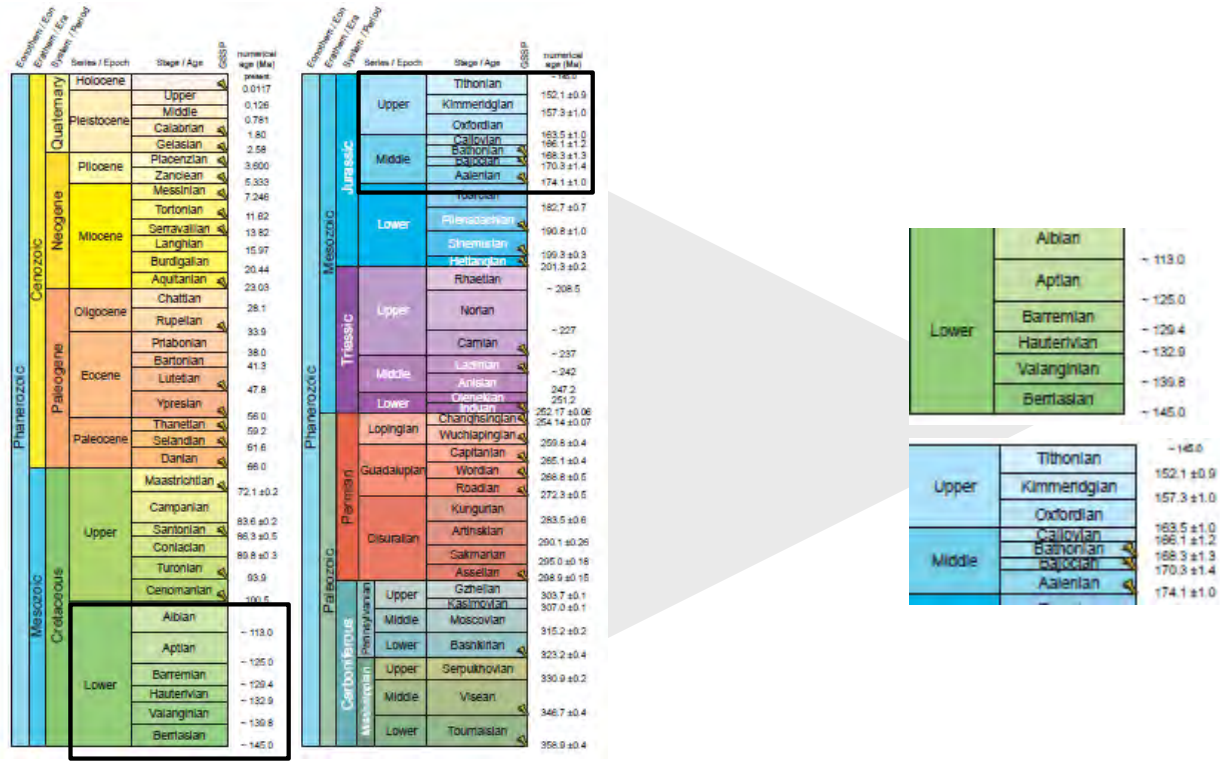

Figure 8. International Chronostratigraphic Chart. Zoom in important ages to present study: Tithonian-Berriasian Ages.

The unit was dated as Berriasian based on dinocysts and correlated with the top of the Farta Pão and Freixial units, both also considered as Berriasian based on foraminifera, ostracods and charophytes, namely by including the foraminifera *Anchispirocyclina lusitanica*, indicating a Tithonian to lowermost Cretaceous age. About 2.5 km to the south of Porto da Calada the unit shows an increase in the proportion of marginal marine beds and a more diverse fossil association, including in the lower levels the bivalve *Pterotrigonia caudata* that indicates the Early Cretaceous. In the magnetostratigraphic study recently conducted in the Porto da Calada section, considering the biostratigraphical constraints, the Tithonian-Berriasian boundary (at the base of magnetozone M18r) was tentatively located at 51-53 m (Figure 9), about 5 m below the limit between the Assenta Mb. and the Porto da Calada Fm.

Figure 9. Escadinha Beach outcrop (north of the Porto da Calada Beach): the line J/K marks the Jurassic-Cretaceous boundary (Salminen et al., 2013), the line A marks the boundary between the Lourinhã Fm. (below) and the Porto da Calada Fm. (above).

Figure 10. Porto da Calada Beach outcrop: the line J/K marks a possible location of Jurassic-Cretaceous boundary. Above this limit were collected the samples PC1 - PC14 and under this limit the samples PC20 – PC27.

The carbonate intercalations of the upper part of the unit (around 20 and 40 m in Figure 12) include laminated marls, and limestones with a marked nodular characteristic resulting from intense *Thalassinoides* ichnofabric, a facies typical of the Farta Pão unit further south (Ramalho, 1971).

The top boundary of the unit is defined by the transition from a mudstone dominated interval to the sandstone-rich with thin micritic and dolomitic layers of the Porto da Calada Formation, marked in detail by a thick sandstone channel body (in accordance with Rey, 1993).

It is difficult to give the unit's exact thickness, since the base is covered and affected by faults, but it can be estimated around 300 m (Wilson, 1979; Hill, 1988). The dominant clay minerals association is illite-smectite (Manuppella et al., 1999).

In detail, the upper carbonate level of the Assenta Mb. in the Porto da Calada section is quite likely the upper tongue of the Freixial Mb. of the Farta Pão Fm. in the Arruda Sub-basin, correlated by Leinfelder & Wilson (1998) with the base of the latest Tithonian T5 sequence of the European Sequence Stratigraphic Chart of Jacquin et al. (1998).

Rey (1993) identified five 3rd order depositional sequences, with late transgressive to high stand intervals represented by carbonate and laminated fine sandstone beds deposited in intertidal plains to internal marine platform. The low stand to early transgressive systems correspond essentially to sandy meandering fluvial channels, linked to estuarine channels and bars, interbedded and cutting the floodplain and intertidal flats (Figure 11). These low energy deposits had developed paleosols, as shown by the *in situ* and the reworked calcrete nodules.

Figure 11. Evidence of marine environment – ripple markers.

Figure 12. Porto da Calada stratigraphic log and M-anomalies. Black (white) indicates normal (reversed) polarity (Salminen, 2013).

4. Sampling and Data Processing

In this section, all the work conducted in the field and in the laboratory will be summarized, and the materials used and procedures executed for each case will be presented.

4.1. Field Work

In the field, a gasoline-powered rock diamagnetic drill (combined with a water pump, to prevent the power drill to overheat) and a magnetic compass to orient the samples were used. The procedure carried was the following:

1. Define the geological limit and start sampling. See Figure 10.

2. Use the gasoline-powered rock diamagnetic drill perpendicular to the rock to mark the spot where the samples will be removed. The rock will be marked with a circumference. About at half the circumference cut the rock to get a sample.[A]

A

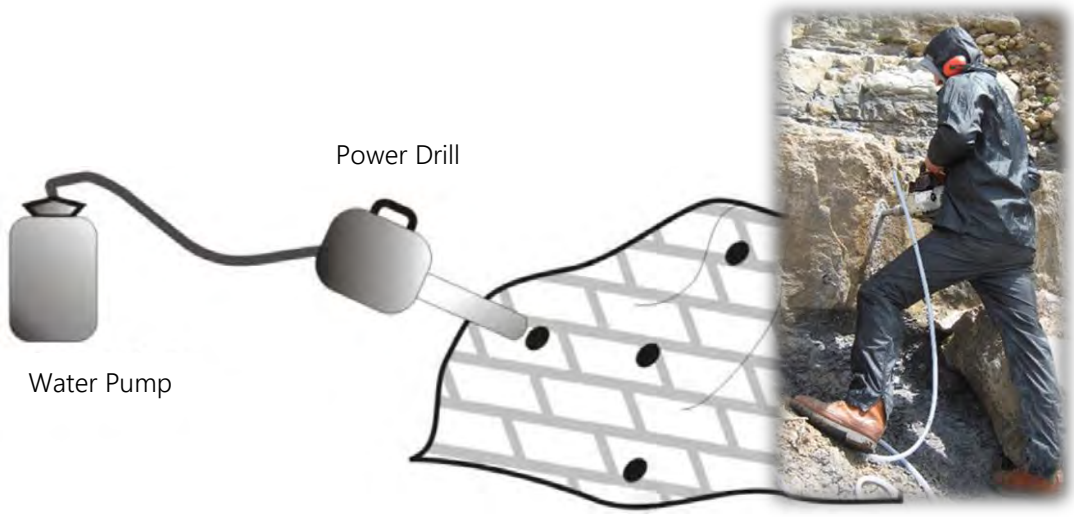

Figure 11. Schematic view and photo of the work conducted in the field.

3. Draw a vertical line on the visible part of the sample with an acetate pen[B] and remove the sample.

B

Figure 12. Example of point 3 of procedure.

4. Use the magnetic compass in the place where the sample was removed to orient it: declination (**Az**) and inclination (**α**).[C]

C

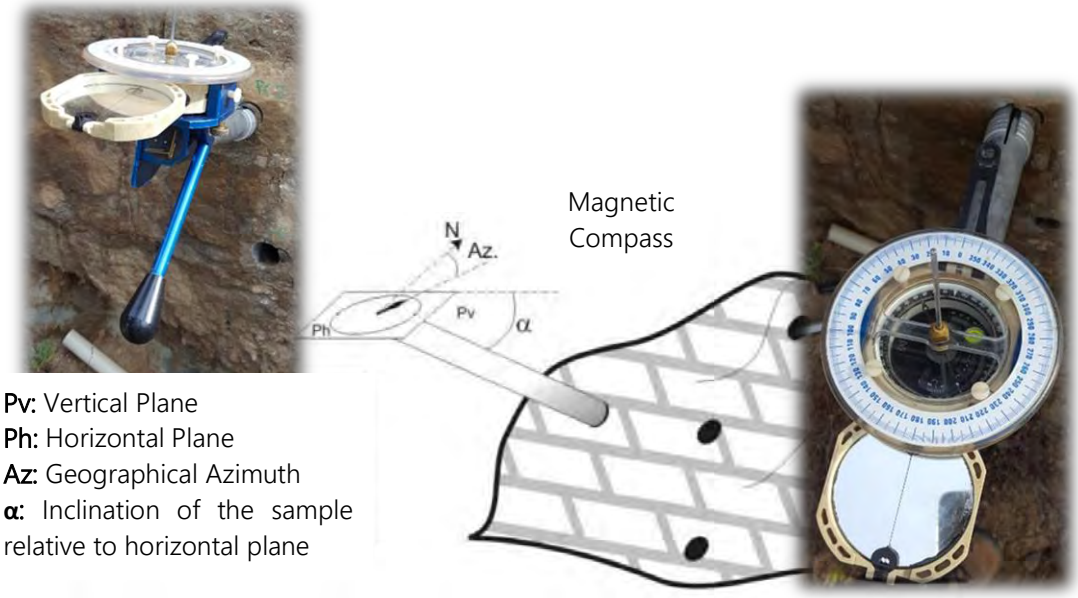

Pv: Vertical Plane
Ph: Horizontal Plane
Az: Geographical Azimuth
α: Inclination of the sample relative to horizontal plane

Figure 14. Schematic view and field photos of the declination and inclination measurement of samples.

5. Mark the sample to identify the top: on the surface, with a vertical line, draw a quarter of the circumference to the left, starting from the bottom. From this point, draw a vertical line along the height of the cylinder and make small arrows directed to the top on one side of the line. On the other side, draw a diagonal line, starting from the top.[D]

D

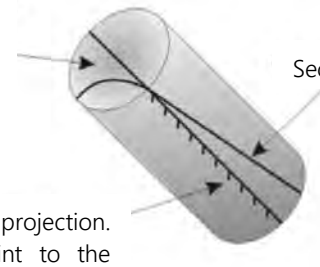

Figure 13. Schematic view of the marks done in the sample after orientation.

6. Identify the sample: write its name on it at least in three different places, along the length of the sample.

4.2. Laboratory Work

In the laboratory the main steps done were: preparing the samples by cutting them into standard paleomagnetic specimens (2:2 cm), and measuring their magnetization.

Note:

The cylindrical shape of every sample is best described by the spherical shape, which is considered in theoretical models.

4.2.1. Sample preparation

To cut the samples, they were firstly measured to see how many specimens could be obtained from each one. They were then cut with an electric saw[1] with two discs separated by 2 cm (Figures 16 and 17).

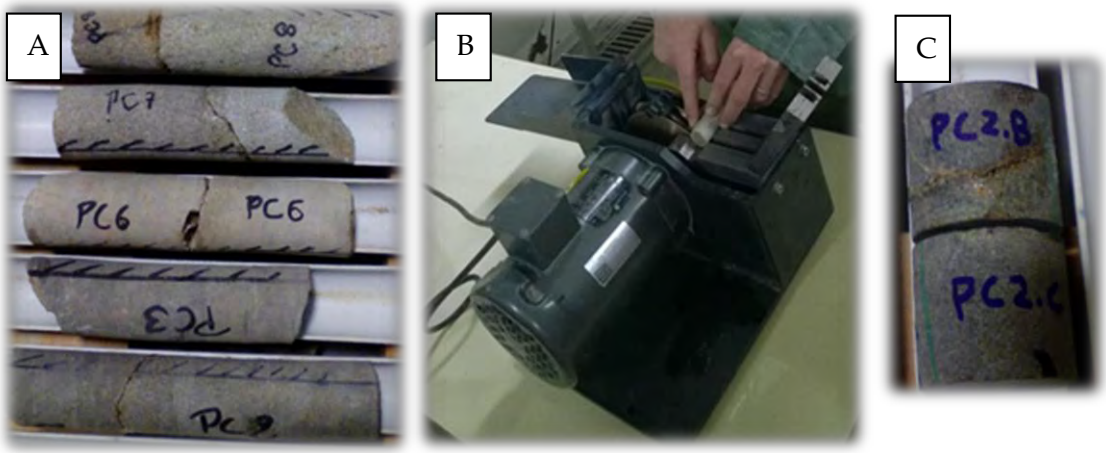

Figure 15. Left: samples; Centre: electric saw; Right: specimens.

Figure 16. Left: all demagnetized specimens; Centre and right: examples of good specimens.

Note:

Put water in the container of the electric saw to prevent it to overheat while it is working.

4.2.2. Demagnetization

The specimens were demagnetized with the AF Demagnetizer LDA-3A (Figure 18) and their magnetization was measured with the Rema6W Software and the Dual Spinner Magnetometer JR-6A (Figure 18), using the following procedure:

1. Start Rema6W software and in *Instrument control* choose the options: *GO ONLINE*, *Normal time*.

2. Use the calibration cylinder[1] to calibrate the magnetometer. Choose options: *Run*, *Calibration*.

3. Identify the specimen with name, declination, inclination and volume (11:15 ccm).[2]

4. Measure the Natural Remanent Magnetization (NRM) with the magnetometer in the four diferent orientations (Figure 20).[3]

5. Use the demagnetizer to remove the magnetization of the specimen in short steps: 2, 4, 6, 8, 12, 15, 20, 25, 30, 40, 50, 60, 80 e 100 mT.[4]

6. Measure magnetization in the same diferent orientations for each step in point 5.[5]

7. Repeat the procedure in points 5. and 6. for all specimens.

Figure 17. AF Demagnetizer LDA-3A (left) and the Dual Spinner Magnetometer JR-6A (right).

Notes:

1. Insert the parameters relative to the calibration cylinder: Standard Magnetization - 6.32 A/m - and Volume - 11.15 ccm. (Figure 19).
2. The volume of the specimen is constant for all of them.
   The inclination and declination measured in the field for each sample is presented in the table below. The samples marked with a ✓ were the samples used to calculate the mean pole.

Table 1. Declination and inclination of each sample measured in the field.

Porto da Calada - 08/04/2016							
Ref.	D (°)	I (°)	Obs.	Ref.	D (°)	I (°)	Obs.
PC1	46	81	✓	PC14	299	87	
PC2	35	80		PC20	80	82	
PC3	70	80	✓	PC21	69	80	
PC6	292	71	✓	PC22	234	46	
PC7	305	75	✓	PC23	90	77	✓
PC8	285	72		PC24	67	74	
PC11	4	83		PC25	65	84	
PC12	15	89		PC26	95	78	
PC13	12	69	✓	PC27	75	86	

3. Before inserting the specimen in the magnetometer, wrap it in cellophane, to prevent small particles to be loose inside the instrument.
4. Insert the following parameters in the demagnetizer command before using it: Time: 20 s; Rate dec.: Medium; Rate inc.: Medium; Slope: Linear. Then, press Start/Stop button.
5. Between each step, it is imperative to *Save Data* and select *New State*.

Figure 18. Calibration cylinder.

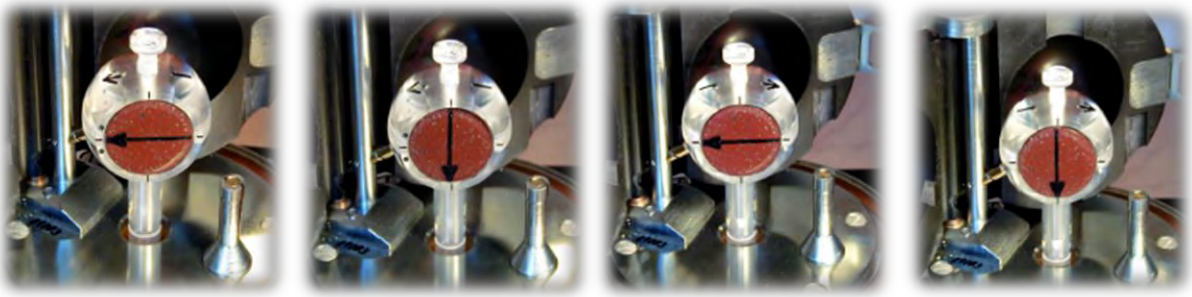

Figure 19. Different positions of the specimens of SPINNER MAGNETOMETER JR6/JR6A User's Manual AGICO.

5. Data Analysis

The analysis of the data obtained in the laboratory was performed with two programs: Remasoft 3.0 and GMAP2012. The first was used to calculate the mean pole of the PC specimens and to compare the magnetization of the samples with the magnetization of the current Porto da Calada pole. The second one was used to compare the obtained pole with the Iberian mean poles. We also used GMAP2012 to rotate the pole of Porto da Calada into African coordinates to compare it with the African mean poles. The procedure was the following:

To calculate the mean poles

1. Start Remasoft to find vectors for ChRM of each specimen.
2. Choose the best data points to get the vectors.
3. Save *C1* component with *APPEND TO FILE* option.
4. Analyze *C1* component in *Group Statistics*.
5. Insert field coordinates and get the results for the mean pole.

To compare the PC pole with the Iberian mean poles

1. Start GMAP2012.
2. In *VGP* open the file *Iberian mean poles.vgp* (medium poles for Iberian Plate for eight time periods).
3. In *Table* add the coordinates of the obtained pole.
4. Click *Draw* and choose the best projection.[1]

To rotate the PC pole to African coordinates and compare it with the African mean poles

1. Save a file in GMAP2012 with the PC pole.
2. In *Euler Rotation* insert the Euler pole to rotate the PC pole from Iberian coordinates to African ones for the age of 130Ma and 151Ma.[2]
3. In *VGP* select *Rotate* and next *Draw* to visualize the rotated PC pole.
4. In *VGP* open the file *T08_SouthAfrica.vgp* (medium poles for African Plate for sixteen time periods).
5. Also, in *VGP* choose *Merge* and next *Draw*.

Notes:

1. By default, GMAP2012 shows the mean poles projected in the South Hemisphere, projecting them using an orthogonal projection.
2. Next, we rotate the Porto da Calada pole to African coordinates to compare it with the African Apparent Polar Wander Path. The Euler Poles used are presented in Table 2. This choice is justified by the age of Tithonian-Berriasian period (~140 Myr).

Table 2. Euler rotations poles for Iberia-Africa.

Longitude (˚)	Latitude (˚)	Angle (˚)	Age (Myr)
-11.44	37.07	15.63	130
-10.02	44.21	19.35	151

6. Results and Discussion

Of the samples collected at Porto da Calada section, 23 were demagnetized under an alternating field and later analyzed with Remasoft, which uses principal component analysis (PCA) and Fisher statistics (Figures 20 to 22). Throughout this analysis, it was clear that some samples were not suitable for further studies, for their magnetization had the same order of magnitude of the sample holder or they did not present stable demagnetization patterns (such as the sample in Figure 22). Consequently, only 13 were selected to obtain the mean pole, which will be discussed further in this work.

When analyzing the demagnetization curves, it was observed that the samples had a remanent coercivity between 7 mT and 25 mT. This indicates that the samples have a low coercivity, and thus are easily remagnetized.

Comparing the samples PC6 (Figure 20) and PC13 (Figure 21), it can be assumed that the magnetic carrier in PC6 sample is magnetite, as it presents a coercivity near 10 mT and it does not fully demagnetize. As for PC13, it is assumed that the magnetic carrier in this sample is hematite, since the sample is still 60% magnetized at 100 mT. In the presence of oxygen, magnetite will oxide, converting to hematite. As such, the magnetic carrier present in the PC6.B sample may be in fact secondary hematite instead of primary magnetite. If hematite was primary, all the samples would present a demagnetization pattern similar to the one in Figure 21. As this is not verified, the hematite present in these samples has a secondary origin. To analyze these samples, it would be best to use thermal demagnetization, in order to reach their Curie temperatures.

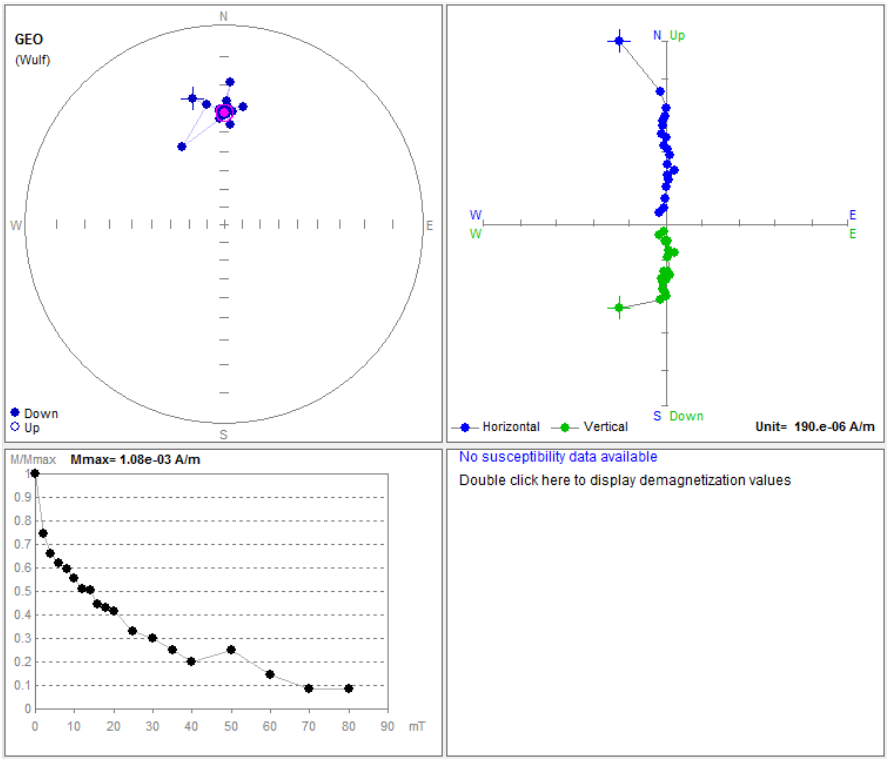

Figure 20. PC6.B specimen. Spherical projection on geographical coordinates is on the top left; the Zijderveld diagram on the top right. The bottom row shows the AF curve on the left; and the magnetic susceptibility on the right (not available).

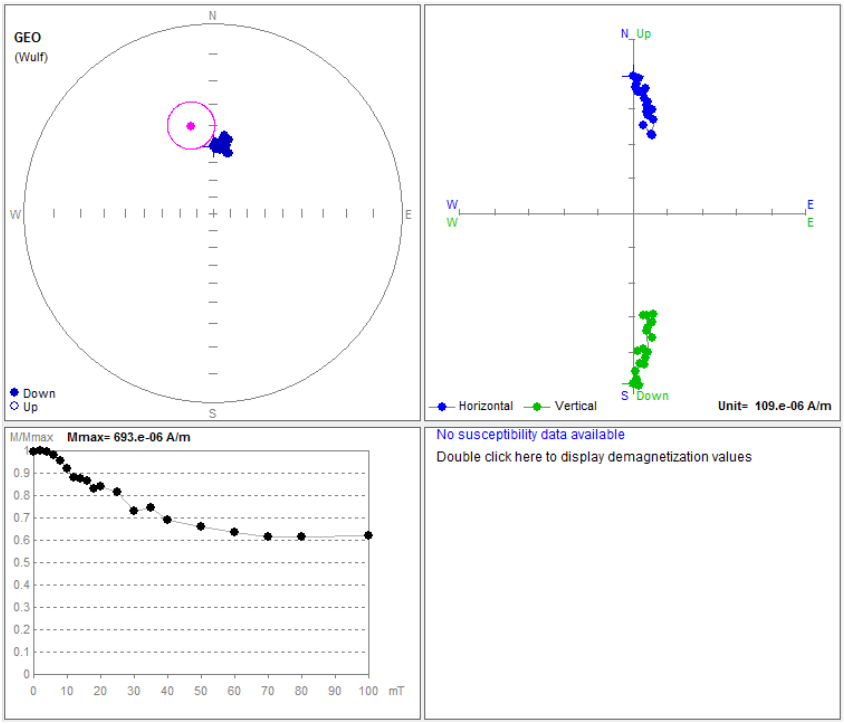

Figure 21. PC13.C specimen. Spherical projection on geographical coordinates is on the top left; the Zijderveld diagram on the top right. The bottom row shows the AF curve on the left; and the magnetic susceptibility on the right (not available).

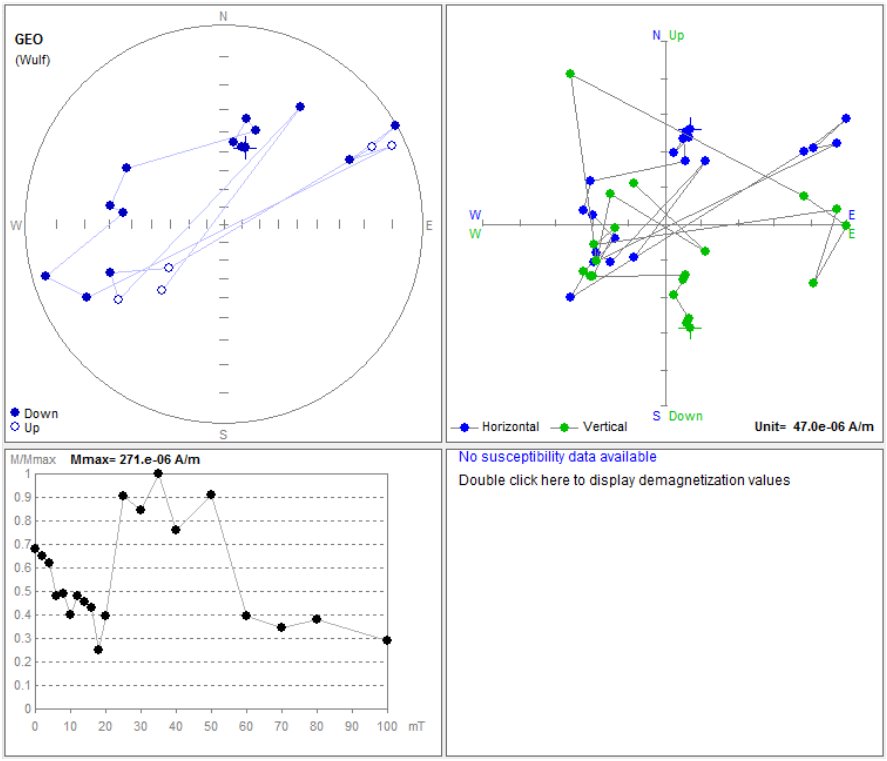

Figure 22. PC25.A specimen. Spherical projection on geographical coordinates is on the top left; the Zijderveld diagram on the top right. The bottom row shows the AF curve on the left; and the magnetic susceptibility on the right (not available).

As previously mentioned, the mean pole was initially calculated using the 13 specimens, for which the demagnetization curve presented a stable pattern. From this 13 specimens, three were subsequently removed due to the lack of proximity to the remaining ones. After their removal, a lower confidence interval - α_{95}- was obtained, which means that the probability of the calculated pole to be located in a certain region increased. This can be seen in Figure 23.

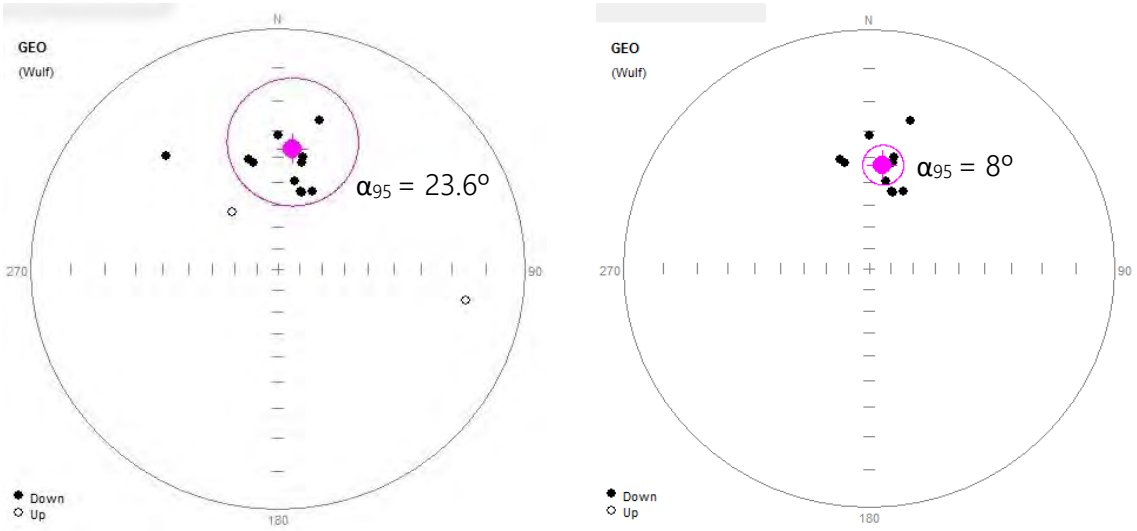

Figure 23. Characteristic remanent magnetization - ChRM (declination and inclination), of the 13 demagnetized specimens - left and of the 10 specimens used to calculate the mean pole - right.

In Table 3 are the inclination and declination values obtained for each specimen as well as for the current magnetic field in Porto da Calada. The magnetization of the 10 specimens with the current direction of Porto da Calada magnetization were also compared. The latter is similar to the specimens' magnetization which indicates that the magnetization of the Porto da Calada specimens is normal (Figure 24).

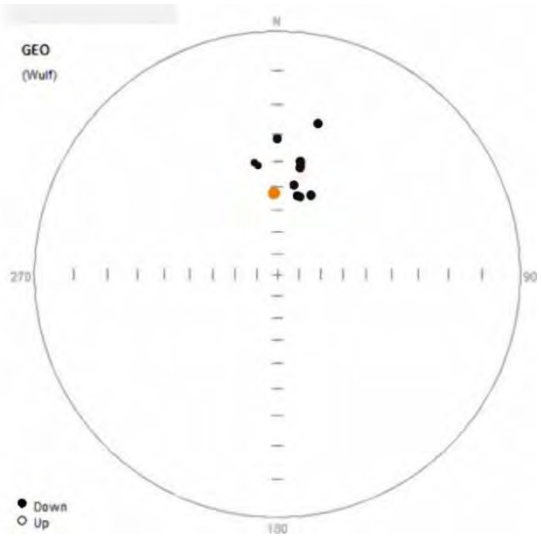

Figure 24. Comparison between the ChRM of the 10 specimens used to calculate the mean pole and the current ChRM of Porto da Calada - orange point.

Table 3. Declination, inclination and maximum angular deviation for the 10 specimens.

Specimen	D (˚)	I (˚)	MAD
PC13.A	15.4	52.9	20.6
PC13.C	345.7	39.3	11.6
PC1.A	10.0	49.1	11.6
PC23.B	12.3	41.3	34.0
PC3.A	23.3	50.9	29.8
PC6.A	347.4	41.0	52.5
PC6.B	359.9	31.6	3.7
PC6.C	12.2	39.1	9.0
PC6.D	16.8	53.3	20.3
PC7.A	14.9	24.6	14.2
Current PC	357.32	53.21	---

To speculate the age of the magnetization of the sediments and find if it is contemporary to the deposition of the sediments or if it was remagnetized throughout its history, the result for the Porto da Calada pole with the Iberian Apparent Polar Wander Path were compared. Then, the Porto da Calada pole was rotated to African coordinates to compare it with the African Apparent Polar Wander Path, using the software GMAP2012. Where there is an overlap of the α_{95} the poles could share the same age. The opposite indicates that the distributions are statistically different, so the poles do not have the same age.

The Porto da Calada section comprises the Tithonian–Berriasian limit, which has about 140 Myr. So firstly the obtained pole was compared with the Iberian APWP (Figure 25). Since there is an overlap of the α_{95} between the obtained Porto da Calada pole and the 70 Myr pole of Iberian APWP, it can be assumed that the magnetization is secondary (rocks were probably remagnetized). Regarding the presence of magnetic inversions, these were not found in the Porto da Calada samples as was expected, based on a study of Salminen et al. (2013).

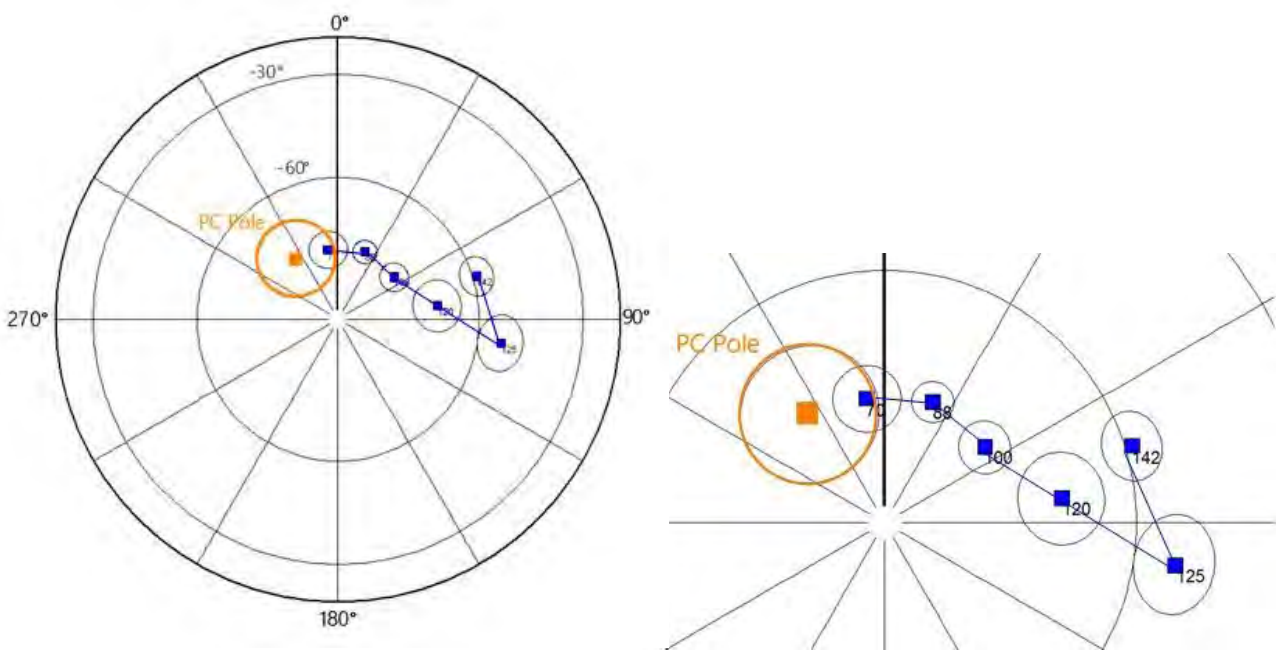

Figure 25. Comparison between the Porto da Calada (orange) pole and the Iberian APWP (blue) for the 142-70 Myr time period. Right figure: zoom.

The new age determinations, combined with previously published data, allows to constrain the duration of the Late Cretaceous alkaline cycle to circa 22 Myr and to define two distinct pulses of alkaline magmatic activity. The first one (94–88 Myr) occurred during the opening of the Bay of Biscay and consequent rotation of Iberia (123–80 Myr; Sibuet et al., 2004) and clusters around the Lisbon area (above N38°20') where it occurs mainly as sills (Foz da Fonte and Paço d'Ilhas). The second pulse lasted from 75 Myr to 72 Myr and corresponds to a more widespread event with scattered occurrences from the Algarve Basin in southernmost Portugal (37°N) to the Lisbon area (39°N) and comprises both intrusive and extrusive complexes. This final pulse is synchronous with the first pulses of tectonic inversion of the Mesozoic basins due to the onset of rapid convergence

between the African and Iberian plates (e.g. Mougenot, 1980; Terrinha, 1998; Rosembaum et al., 2002). The Sintra granite laccolith has an age (79 Myr) between these two pulses of magmatism. The similar ages obtained for the lower volume of alkaline magmatism intruding the opposite rifted and thinned margins of the Iberian plate (105–69 Myr in the Pyrenees and Catalan ranges, Fabriès et al., 1998; Montigny et al., 1986; Solé et al., 2003) suggest a relationship between the Late Cretaceous magmatism and the changes in plate kinematics and seafloor spreading geometry contemporaneous with the opening of the Bay of Biscay (Miranda et al., 2009).

Thus, the most likely origin of remagnetization is the intrusion phase of the Volcanic Complex of Lisbon (VCL). This remagnetization may have been thermal or chemical. It is probably the latter due to circulation of hydrothermal fluids through the cracks and faults that may have formed during magmatic intrusions.

The results obtained for the Porto da Calada pole rotation to African coordinates are presented in Figures 26 (151 Myr) and 27 (130 Myr).

Looking at Figure 26, there is an overlap of the α_{95} between the Porto da Calada pole obtained and several poles of different ages of African APWP. This means that there is a probability of 95% of the Porto da Calada pole to assume any of these ages. Once again, as the Porto da Calada pole is not over the 140 Myr age, the rocks were probably remagnetized. Observing Figure 27, it is possible to conclude the same as in Figure 26 and increase the trustworthiness of what was assessed when the Porto da Calada pole was compared to the Iberian APWP (Figure 25).

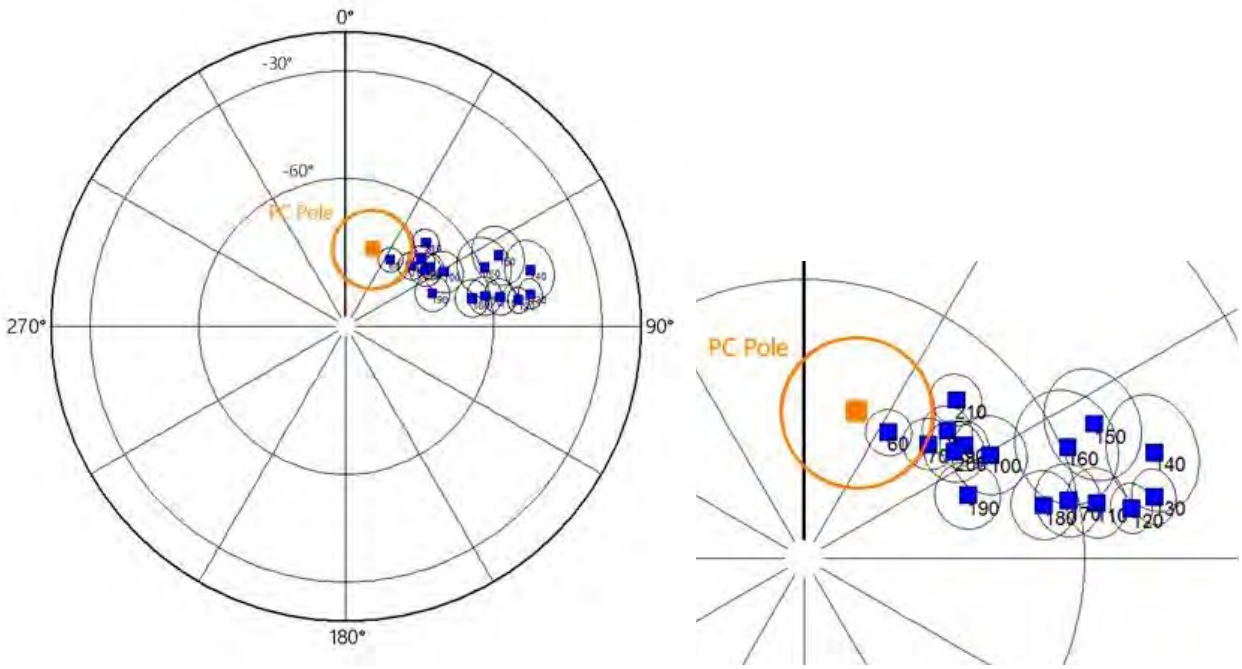

Figure 26. Comparison between the Porto da Calada (orange) pole (rotate with Euler Pole of 151 Myr) and the African APWP (blue) for the 210-60 Myr time period. Right figure: zoom.

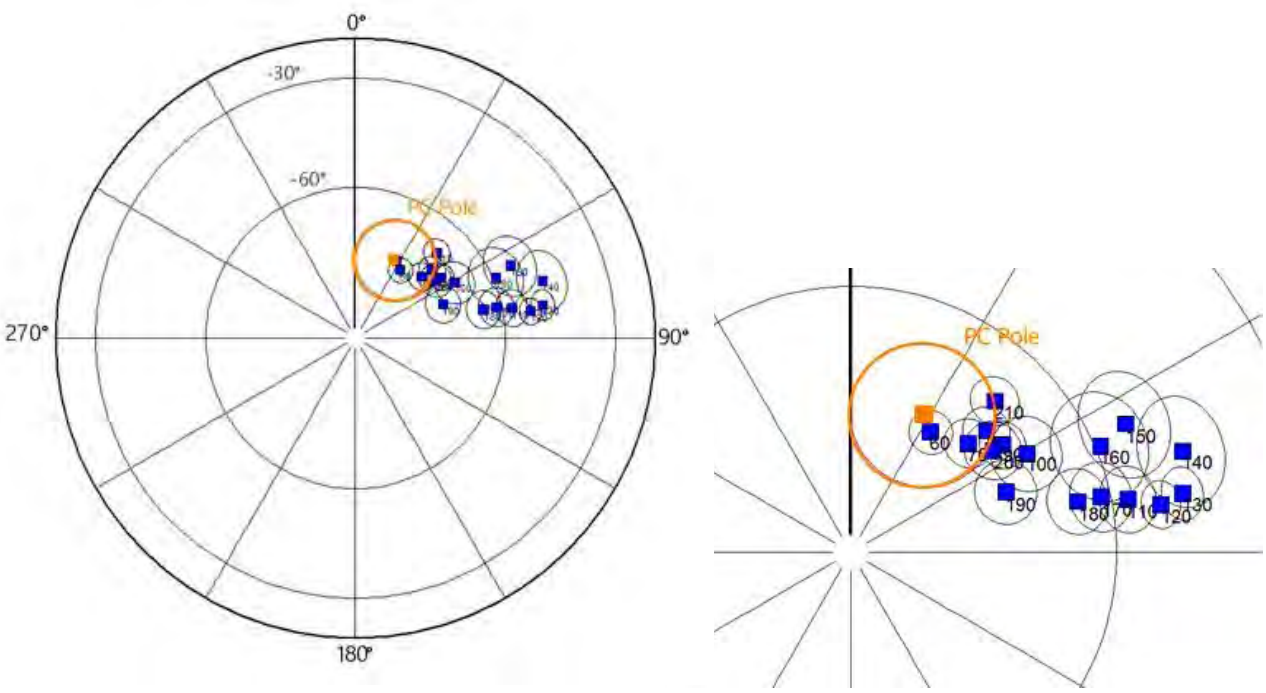

Figure 27. Comparison between Porto da Calada (orange) pole (rotate with Euler Pole of 130 Myr) and African APWP (blue) for the 210-60 Myr time period. Right figure: zoom.

7. Conclusions

Based on the analyses carried on Porto da Calada samples, a paleomagnetic pole with 70 Myr was obtained, which means that, since the studied section has approximately 140 Myr, the samples have been remagnetized. Furthermore, no field inversion was found, due to one of the following reasons: either the magnetic field inversions really do not exist in this section, or the demagnetization process that was used in this work was not the most adequate to study these samples.

8. References

BUTLER, R. (2004). *Paleomagnetism: Magnetic Domains to Geologic Terranes*. Electronic Edition, 248 pp.

DINIS, J. L., REY, J., CUNHA, P. P., CALLAPEZ, P. M., REIS, R. P. (2008). *Stratigraphy and allogenic controls on the western Portugal Cretaceous: An updated synthesis*. Cretaceous Research, 29, pp. 772–780.

FABRIÈS, J., LORAND, J.-P., BODINIER, J.-L. (1998). *Petrogenetic evolution of orogenic lherzolite massifs in the central and western Pyrenees*. Tectonophysics 292, pp. 145–167.

FONT, E., *Trabalhos práticos em magnetismo de rocha – disciplina de Geomagnetismo*. Laboratório de Paleomagnetismo e Magnetismo de Rocha.

FÜRSICH, F. T., WERNER, W. (1986). *Benthic associations and their environmental significance in the Lusitanian Basin (Upper Jurassic, Portugal)*. Neues Jahrbuch für Geologie und Paläontologie, Abhandlungen, 172, pp. 271-329.

HILL, G. (1989). *Distal alluvial fan sediments from the Upper Jurassic of Portugal: controls on their cyclicity and channel formation*. Journal of the Geological Society, 146(3), pp. 539-555.

IPMA, Instituto Português do Mar e da Atmosfera, *Geomagnetism*. https://www.ipma.pt/en/enciclopedia/geofisica/geomagnetismo/index.html

JACQUIN, T., DARDEAU, G., SURLET, C., DE GRACIANSKY, P.-C., HANTZPERGUE, P. (1998). *The North Sea Cycle: an overview of 2nd order transgressive/regressive facies cycles in Western Europe*. In: de Graciansky, P.-C. Hardenbol, J. Jacquin, T. & Vail, P.R. (Eds.), Mesozoic and Cenozoic Sequence Stratigraphy of European Basins. SEPM (Society for Sedimentary Geology) Special Publication, 60, pp. 397-410.

LEINFELDER, R. R. (1986). *Facies, Stratigraphy, and Paleogeographic Analysis of Upper? Kimmeridgian to Upper Portlandian Sediments in the Environs of Arruda Dos Vinhos, Estremadura, Portugal*. München. Münchner Geowissenschaftliche Abhandlungen, 7, 215 pp.

LEINFELDER, R. R., WILSON, R. C. L. (1998). *Third order Sequences in an Upper Jurassic Rift-Related Second Order Sequence*, Central Lusitanian Basin, Portugal. In: P.-C. de Graciansky, J. Hardenbol, T. Jacquin & P. Vail (Eds.) Mesozoic and Cenozoic Sequence Stratigraphy of European Basins. SEPM (Society for Sedimentary Geology) Special Publication, 60, pp. 507-525.

MANUPPELLA, G. (COORD.), ANTUNES, M. T., PAIS, J., RAMALHO, M. M., REY, J. (1999). Notícia Explicativa da Folha 30-A, Lourinhã. Instituto Geológico e Mineiro, Lisbon, 83 pp.

MATEUS, O. (2006). *Late Jurassic dinosaurs from the Morrison Formation (USA), the Lourinhã and Alcobaça formations (Portugal), and the Tendaguru Beds (Tanzania): a comparison*. New Mexico Museum of Natural History and Science Bulletin, 36, pp. 223-231.

MIRANDA, J. M. (2009). *Introdução ao Geomagnetismo*. Aulas de Geomagnetismo do Departamento de Engenharia Geográfica, Geofísica e Energia da Faculdade de Ciências da Universidade de Lisboa.

MIRANDA, R. (2009). *Age constraints on the Late Cretaceous alkaline magmatism on the West Iberian Margin*, Cretaceous Res., vol. 30, no. 3, pp. 575-586.

MONTIGNY, R., AZAMBRE, B., ROSSY, M., THUIZAT, R. (1986). *Kr-Ar study of cretaceous magmatism and metamorphism in the Pyrenees: age and length of rotation of the Iberian Peninsula*. Tectonophysics 129, pp. 257–273.

MOUGENOT, D. (1980). *Une phase de compression au Crétacé terminal à l'Ouest du Portugal: quelques arguments*. Boletim da Sociedade Geológica de Portugal XXII, pp. 233–239.

MYERS, T. S., TABOR, N. J., JACOBS, L. L., MATEUS, O. (2012a). *Estimating soil pCO2 using paleosol carbonates: implications for the relationship between primary productivity and faunal richness in ancient terrestrial ecosystems*. Paleobiology, 38(4), pp. 585-604.

MYERS, T. S., TABOR, N. J., JACOBS, L. L., MATEUS, O. (2012b). *Palaeoclimate of the Late Jurassic of Portugal: Comparison with the Western United States*. Sedimentology, 59(6), pp. 1695–1717.

NERES, M. (2013). *Magnetic studies of the late cretaceous magmatism in Portugal: from Iberian plate kinematics to magnetic fabrics*, Ph.D. thesis, Universidade de Lisboa and Université de Toulouse.

OGG J. G., HINNOV L. A., HUANG C. (2012). *Cretaceous*. In: Gradstein, F. M., Ogg, J. G., Schmitz, M.D. & Ogg G. M., The Geologic Time Scale 2012, vol. 2, Elsevier, Oxford, pp. 793-853.

RAMALHO, M. M. (1971). *Contribution à l'étude micropaléontologique et stratigraphique du Jurassique Superieur et Crétacé Inferieur des environs de Lisbonne (Portugal)* - Memórias dos Serviços Geológicos de Portugal, Nova Série 19, 212 pp.

REY, J. (1972). *Recherches géologiques sur le Crétacé inférieur de l'Estremadura (Portugal)*. Memórias dos Serviços Geológicos de Portugal, Nova Série 21, 477 pp.

REY, J. (1993). *Les unités lithostratigraphiques du Grupe de Torres Vedras (Estremadura, Portugal)*. Comunicações do Instituto Geológico e Mineiro, 79, pp. 75-85.

REY, J., DINIS, J. L., CALLAPEZ, P., CUNHA, P. P. (2006). *Da rotura continental à margem passiva. Composição e evolução do Cretácico de Portugal*. Cadernos de Geologia de Portugal, Ed. INETI, Lisbon, 75 pp.

ROSEMBAUM, G., LISTER, G.S., DUBOZ, C. (2002). *Relative motions of Africa, Iberia and Europe during Alpine orogeny*. Tectonophysics 359, pp. 117–129.

SALMINEN J. *et al* (2014). Preliminary Magnetostratigraphy for the Jurassic–Cretaceous Transition in Porto da Calada, Portugal.

SIBUET, J.C., SCRIVASTAVA, S., SPAKMAN, W. (2004). *Pyrenean orogeny and plate kinematics*. Journal of Geophysical Research 109, B8.

SOLÉ , J., PI, T., ENRIQUE, P. (2003). *New data on the Late Cretaceous alkaline magmatism of the northeast Iberian Peninsula*. Cretaceous Research 24, pp. 135–140.

SPINNER MAGNETOMETER JR6 / JR6A User's Manual Instrument for measuring remanent magnetization (2007). AGICO Advanced Geoscience Instruments Co. Brno Czech Republic.

TERRINHA, P. (1998). *Structural Geology and Tectonic Evolution of the Algarve Basin, South Portugal*. Imperial College, University of London, PhD Thesis.

WILSON, R. C. L. (1979). *A reconnaissance study of Upper Jurassic sediments of the Lusitanian Basin*. Ciências da Terra, 5, pp. 53-84.

ZBYSZEWSKI, G., ALMEIDA, F. M., ASSUNÇÃO, C. T. (1955). *Carta Geológica de Portugal à escala 1: 50000. Notícia explicativa da folha 30-C Torres Vedras*. Serviços Geológicos de Portugal, Lisbon, 33 pp.

9. Appendix

Figure 28. Specimens analyzed in this study. Spherical projection on geographical coordinates is on the top left; the Zijderveld diagram on the top right. The bottom row shows the AF curve on the left; and the magnetic susceptibility on the right (not available).

Figure 29. Geological Map of Torres Vedras, Portugal. Black box indicates Porto da Calada Section.

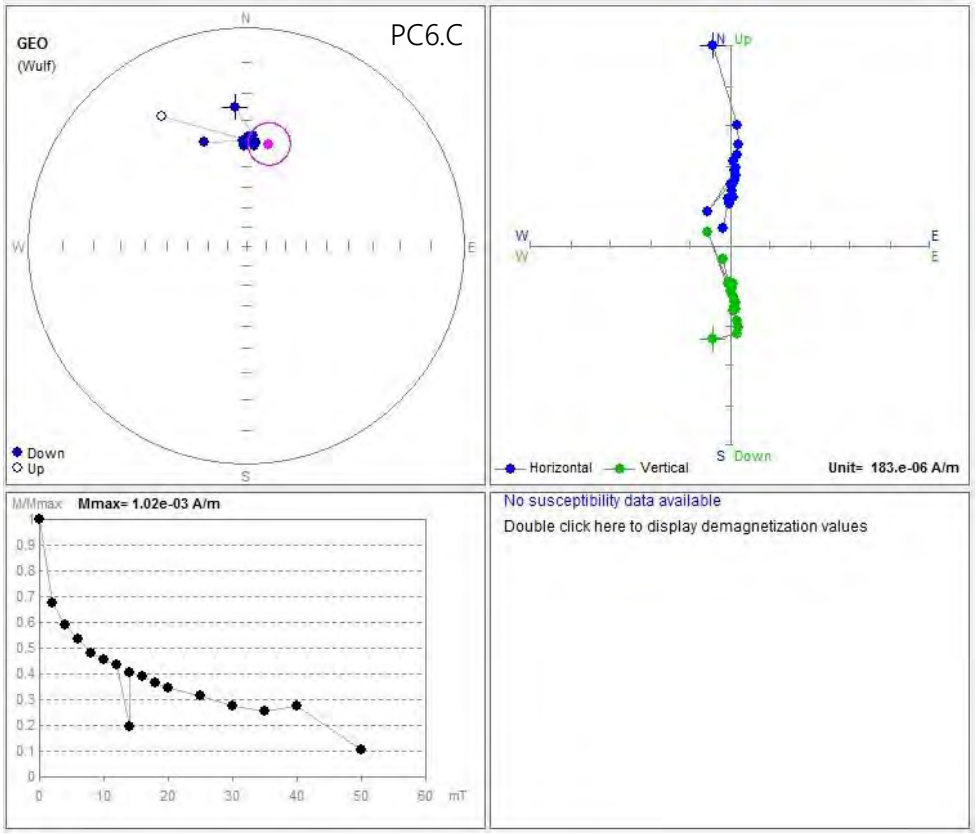
PC6.C
GEO
(Wulf)
N
W
E
S
Down
Up
N Up
W
W
E
E
S Down
Horizontal
Vertical
Unit= 183.e-06 A/m
M/Mmax
Mmax= 1.02e-03 A/m
0.9
0.8
0.7
0.6
0.5
0.4
0.3
0.2
0.1
0
0
10
20
30
40
50
60
mT
No susceptibility data available
Double click here to display demagnetization values

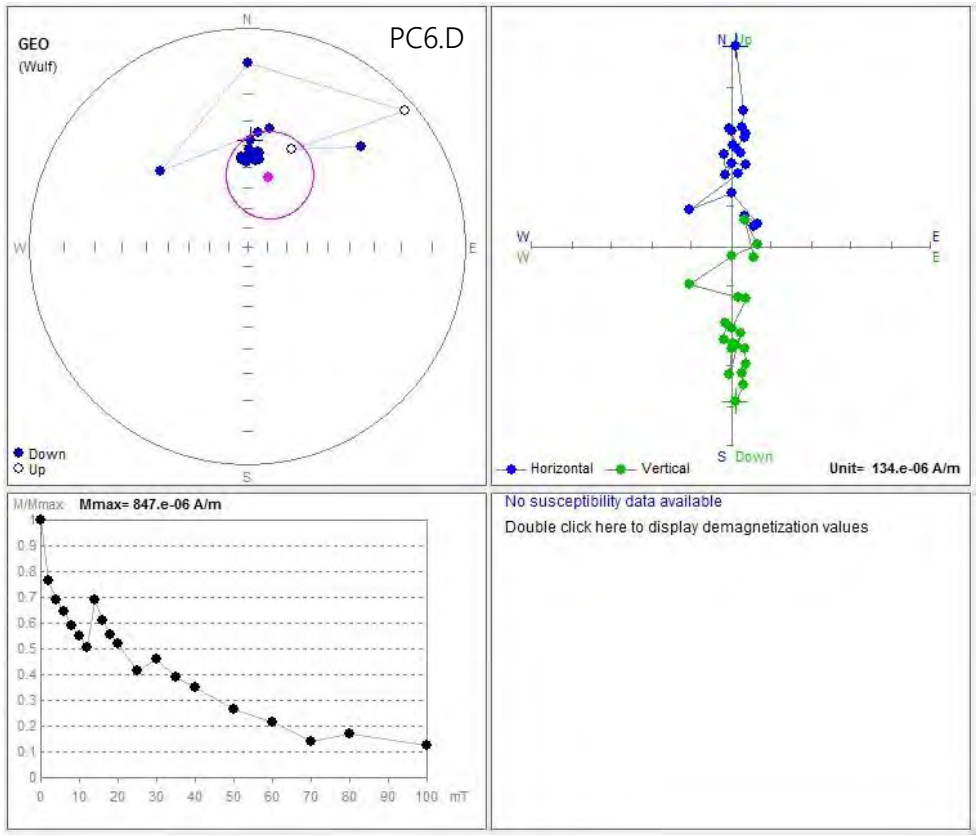
PC6.D
GEO
(Wulf)
N
W
E
S
Down
Up
N Up
W
W
E
E
S Down
Horizontal
Vertical
Unit= 134.e-06 A/m
M/Mmax
Mmax= 847.e-06 A/m
0.9
0.8
0.7
0.6
0.5
0.4
0.3
0.2
0.1
0
0
10
20
30
40
50
60
70
80
90
100
mT
No susceptibility data available
Double click here to display demagnetization values

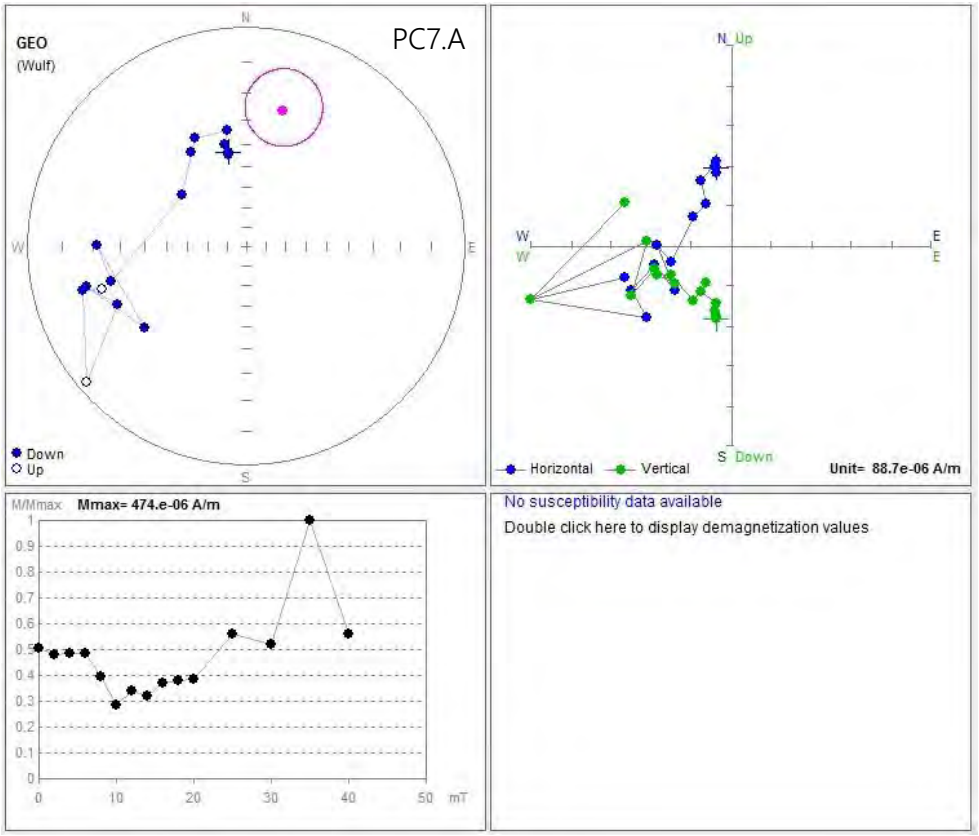
GEO
(Wulf)
PC7.A
N
W
E
S
Down
Up
N_Up
S_Down
Horizontal
Vertical
Unit= 88.7e-06 A/m
M/Mmax
Mmax= 474.e-06 A/m
mT
No susceptibility data available
Double click here to display demagnetization values

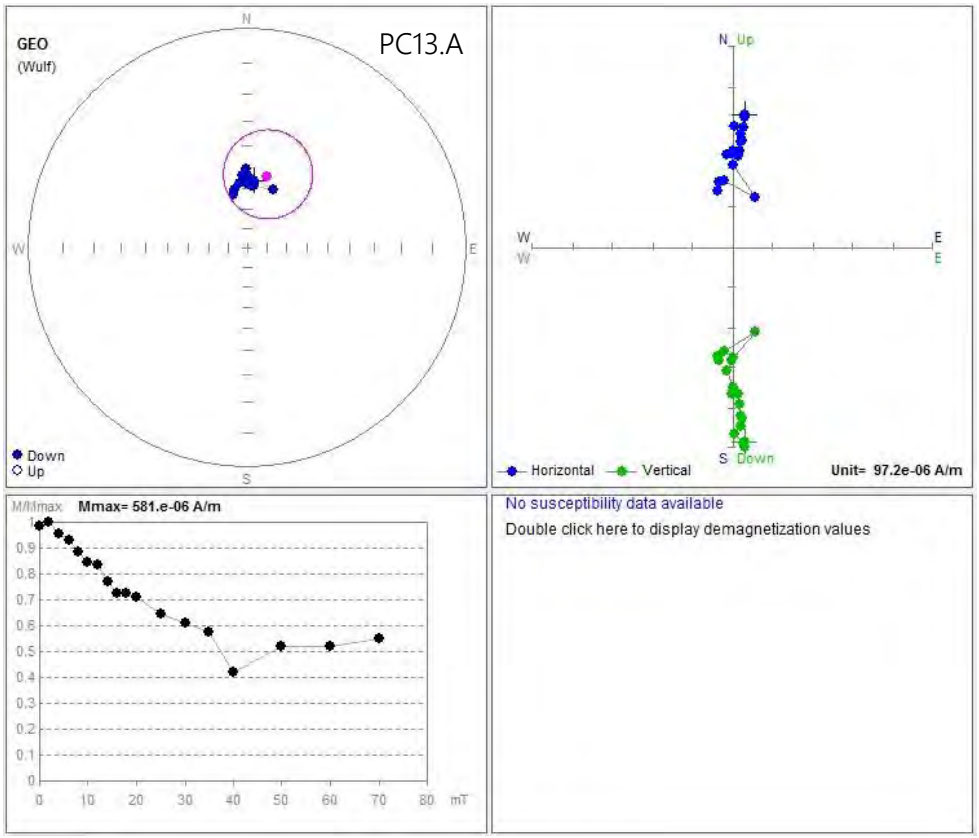
GEO
(Wulf)
PC13.A
N
W
E
S
Down
Up
N_Up
S_Down
Horizontal
Vertical
Unit= 97.2e-06 A/m
M/Mmax
Mmax= 581.e-06 A/m
mT
No susceptibility data available
Double click here to display demagnetization values

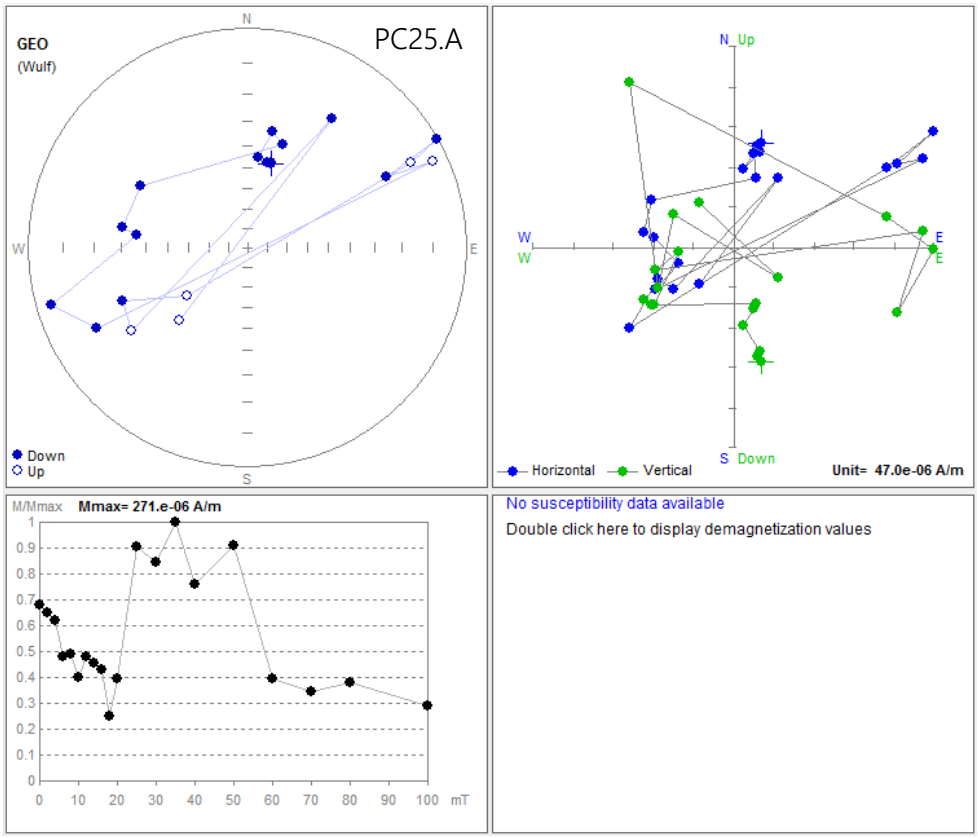
GEO
(Wulf)
PC25.A
N
W
E
S
Down
Up
N_Up
W
W
E
E
S Down
Horizontal
Vertical
Unit= 47.0e-06 A/m
M/Mmax
Mmax= 271.e-06 A/m
0 10 20 30 40 50 60 70 80 90 100 mT
No susceptibility data available
Double click here to display demagnetization values

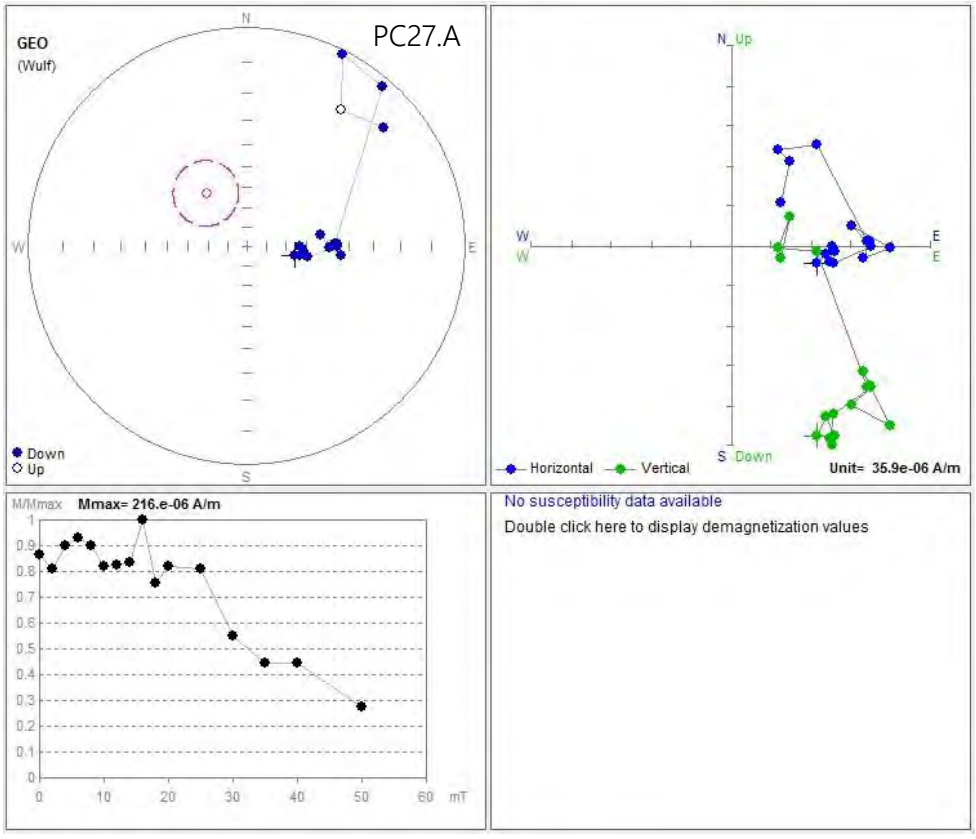
GEO
(Wulf)
PC27.A
N
W
E
S
Down
Up
N_Up
W
W
E
E
S Down
Horizontal
Vertical
Unit= 35.9e-06 A/m
M/Mmax
Mmax= 216.e-06 A/m
0 10 20 30 40 50 60 mT
No susceptibility data available
Double click here to display demagnetization values

30A 30C 30D 34A

DIRECÇÃO GERAL DE MINAS E SERVIÇOS GEOLÓGICOS

SERVIÇOS GEOLÓGICOS

CARTA GEOLÓGICA DE PORTUGAL

30C

TORRES VEDRAS

Escala de 1:50.000

Equidistancia das curvas de nível 25 metros